JOURNAL OF SOLID STATE CHEMISTRY 109, 372–383 (1994)

Crystal Structure and Metal–Semiconductor Transition of the $Bi_{2-x}Ln_xRu_2O_7$ Pyrochlores (Ln = Pr–Lu)

T. Yamamoto,*[,1] R. Kanno,†[,2] Y. Takeda,* O. Yamamoto,* Y. Kawamoto,† and M. Takano‡

*Department of Chemistry, Faculty of Engineering, Mie University, Tsu, Mie-ken, 514 Japan; †Department of Chemistry, Faculty of Science, Kobe University, Kobe, Hyogo-ken, 657 Japan; and ‡Institute for Chemical Research, Kyoto University, Uji, Kyoto-fu, 611 Japan

Received February 22, 1993; in revised form May 25, 1993; accepted September 15, 1993

The quaternary pyrochlore ruthenates, $Bi_{2-x}Ln_xRu_2O_7$ (Ln = Pr–Lu), have been synthesized and characterized by X-ray Rietveld structure refinement and electrical conductivity measurements. Room temperature resistivities increase with x, and a change from metallic to semiconducting behavior is observed between $x = 1.2$ and 1.4. In this composition region, smooth change from metallic to semiconducting behavior was observed at 40–80 K for the Pr–Sm systems, whereas no change was observed for the Dy and Y systems. Lattice parameters increase with x in the systems with larger rare earth cations (Pr, Nd), and decrease with x in the systems with smaller rare earth cations (Sm, Dy). However, the room-temperature structure analysis indicated similar structural changes in these solid solutions; the Ru–O bond length in the RuO_6 octahedra increases, the distortion of the RuO_6 octahedra increases, and the bend in the RuO_6 zig-zag chains increases with increasing Ln contents. This corresponds to the change from metallic to semiconducting behavior around $x = 1.2$–1.4. The RuO_6 octahedra distortion and the bend in the RuO_6 zig-zag chains increase in the order Lu → Pr. The semiconductor–metal transition is discussed from the structural changes.

INTRODUCTION

The pyrochlore ruthenates are technologically important materials as catalysts (1), electrocatalysts (2), and conducting components in thick-film resistors (3–5). Their electronic properties are of intrinsic interest, since the Ru : 4d electrons are on the borderline between localized and itinerant behavior. For example, the bismuth ruthenate $Bi_2Ru_2O_7$ and the lead ruthenate $Pb_2Ru_2O_{6.5}$ are metallic Pauli paramagnets with a nearly temperature-independent resistivity, whereas the rare-earth ruthenates $Ln_2Ru_2O_7$ (Ln = Pr–Lu) and $Y_2Ru_2O_7$ are all semiconductors with a spontaneous ruthenium atomic moment (6–8). The electronic structure of the pyrochlore has recently been studied for $Pb_2Ru_2O_{6.5}$ and $Bi_2Ru_2O_7$ using the pseudofunction method (9); the unoccupied Pb or Bi 6p states are significantly closer to E_F and contribute to their metallic conductivity by mixing with the Ru 4d state via the framework oxygen.

While the conduction mechanisms of the ternary and quaternary ruthenate pyrochlores have been studied, the relationship between their electronic and crystal structures is not quite well understood. In previous studies, we have shown that the X-ray Rietveld refinement technique provides a powerful proof into the structural studies (10–13). We have clarified the structural changes in the quaternary pyrochlore ruthenates, $Bi_{2-x}Y_xRu_2O_7$, the end members of which are, respectively, a metal and an insulator (13). In this system, (i) the Ru–O bond length in the RuO_6 octahedra increases, (ii) the distortion of the RuO_6 octahedra increases, and (iii) the bend in the RuO_6 zigzag chains increases with increasing Y^{3+} contents. These variations affect the Ru–O overlap integrals, leading to the transition from metallic to semiconducting state. The structural changes in the pyrochlores are closely related to their electrical properties.

Since the strength of the Ln–O interaction is expected to decrease with increasing basicity or increasing size of the Ln atom, i.e., in the order Lu → La across the rare-earth series, the pyrochlore with rare-earth series could provide a variety in both structural parameters, such as the B–O bond length and the BO_6 distortion, and their electrical properties. For example, molybdenum pyrochlores, $Ln_2Mo_2O_7$, with Ln = Tb–Yb, are semiconductors with quasi-localized 4d^2 electrons; Ln = Gd is a highly correlated metal or semimetal and Ln = Nd and Sm show more normal behavior consistent with a broader Mo–O π^* band (14). On the other hand, the quaternary pyrochlore ruthenates $Ln_2Ru_2O_7$ (Ln = Pr–Lu) show semiconducting properties (15). The solid solutions, $Bi_{2-x}Ln_xRu_2O_7$, have been synthesized by Ehmann and Kemmler-Sack (16) for Ln = Sm–Lu, and by Goodenough *et al.* for Ln = Gd (17), respectively; these systems show metallic-to-semiconducting property change with composition. Later, the transition in the latter system was studied by photoelectron spectroscopy (18). However, no structural data were

[1] Present address: Central Research Institute of Electric Power Industry, Yokosuka, 240-01, Japan.

[2] To whom correspondence should be addressed.

0022-4596/94 $6.00

reported for the stoichiometric $Ln_2Ru_2O_7$ nor for their solid solutions with $Bi_2Ru_2O_7$. Further, these solid solutions might be expected to have a variety in electrical and structural properties in the boundary regime between metallic and semiconducting state. In the present study, we synthesized the solid solutions, $(Bi_{2-x}Ln_x)Ru_2O_7$ (Ln = Pr–Lu). The relationship between the crystal structure and electrical properties is discussed.

EXPERIMENTAL

The ternary oxides $A_2Ru_2O_7$ (A = Bi, Pr–Lu) and the quaternary oxides $Bi_{2-x}Ln_xRu_2O_7$ (Ln = rare earth) were prepared by heating appropriate molar ratios of RuO_2, Bi_2O_3, and Ln_2O_3 (RuO_2: Furuuchi Chemicals. Ltd., >99.99% purity; Bi_2O_3, Gd_2O_3: Nakarai Chemicals. Ltd., >99.9% purity; Pr_6O_{11}, Sm_2O_3, Eu_2O_3, Dy_2O_3, Er_2O_3, Yb_2O_3, Lu_2O_3: Shinetsu Chemical. Co. Ltd., >99.9% purity; Nd_2O_3: Mitsuwa Chemicals. Co. Ltd., >99.9% purity). The starting materials were dried for 2 days in air at 773 K for RuO_2 and at 1273 K for Ln_2O_3 and Bi_2O_3. They were weighed, mixed, and pelletized in a nitrogen-filled glove box, and put into a platinum tube to avoid a reaction between silica tubes and the samples. The platinum tube was then sealed in an evacuated silica tube and heated at 773 K for 12 hr and at 1173–1473 K for 30–40 hr with regrinding between successive firings. The loss of ruthenium was thus minimized by the above reaction procedure.

X-Ray diffraction (XRD) patterns of the powdered samples were obtained with a high-power X-ray diffractometer (Rigaku RAD 12kW). The focusing graphite monochromater equipped after the samples was used for employing Cu$K\alpha$ radiation. Diffraction data were collected for 2 s at each 0.02° step width over a 2θ range from 10 to 100° at room temperature. The structural parameters were refined by Rietveld analysis with the computer program RIETAN provided by Izumi (19). Reflection positions and intensities were calculated for both Cu$K\alpha_1$ and Cu$K\alpha_2$ with a factor of 0.5 applied to the latter's calculated integrated intensities. A pseudo-Voigt profile function was used; the mixing parameter γ was included in the least-squares refinement.

Electrical resistivities were measured with sintered materials with dimensions of approximately 2 × 2 × 10 mm. The data were obtained by a four-probe method in the temperature range $15 \leq T \leq 300$ K using a CHINO US-36 electrical conductivity measurement system. The temperature was monitored with a calibrated carbon-glass thermometer mounted near the sample. Magnetic susceptibility was measured by a SQUID magnetometer (Quantum Design, MPMS2) between 5 and 350 K. The sign and the magnitude of applied magnetic field were determined with granular Pb metal.

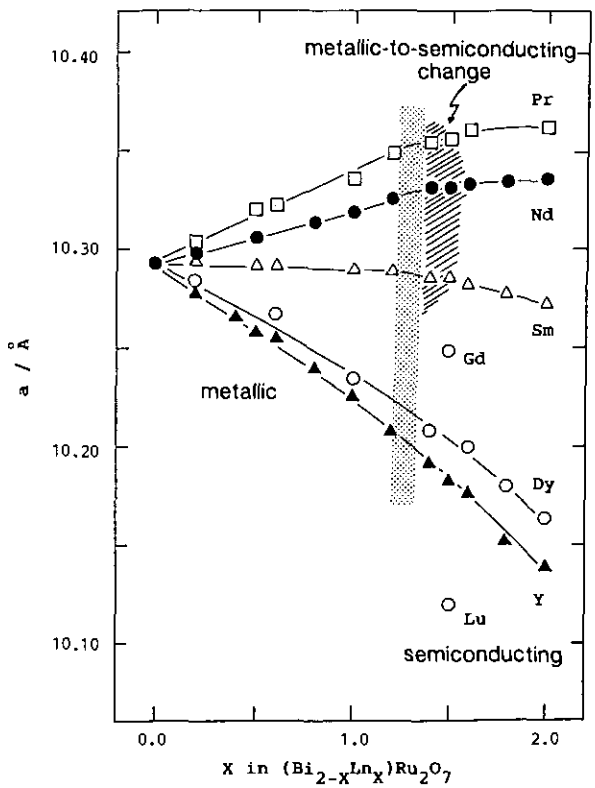

FIG. 1. Composition dependence of lattice parameters for $Bi_{2-x}Ln_xRu_2O_7$.

RESULTS AND DISCUSSION

Synthesis

Monophasic properties of the pyrochlore structure were obtained for the quaternary ruthenates, $Bi_{2-x}Ln_xRu_2O_7$ (Ln = Pr, Nd, Sm, Dy), for the whole range of solid solution; the firing temperature required to produce a single-phase material increased from 1223 to 1573 K with increasing Ln content. Monophasic $Bi_{0.5}Ln_{1.5}Ru_2O_7$ (Ln = Gd, Eu, Lu) were also prepared in the present study at a firing temperature of 1373 K. Figure 1 shows composition dependence of the lattice parameters, after Rietveld refinement, for $Bi_{2-x}Ln_xRu_2O_7$ ($0 \leq x \leq 2.0$), together with the parameters for $Bi_{2-x}Y_xRu_2O_7$ reported previously (13). The lattice parameters increase with x for $Bi_{2-x}Ln_xRu_2O_7$ (Ln = Pr, Nd), while for $Bi_{2-x}Ln_xRu_2O_7$ (Ln = Sm, Dy, Y), the parameters decrease with x. This might correspond to the difference in ionic radii between Bi and Ln ions (Bi^{3+}: r = 1.11 Å; Pr^{3+}: r = 1.14 Å; Nd^{3+}: r = 1.12 Å; Sm^{3+}: r = 1.09 Å; Dy^{3+}: r = 1.03 Å; Y^{3+}: r = 1.015 Å) (20). The lattice parameters vs composition curves do not obey Vegard's Laws; gradual slope changes are observed at $1.0 \leq x \leq 2.0$. Cox *et al.* reported a slope change in the lattice parameter curve at

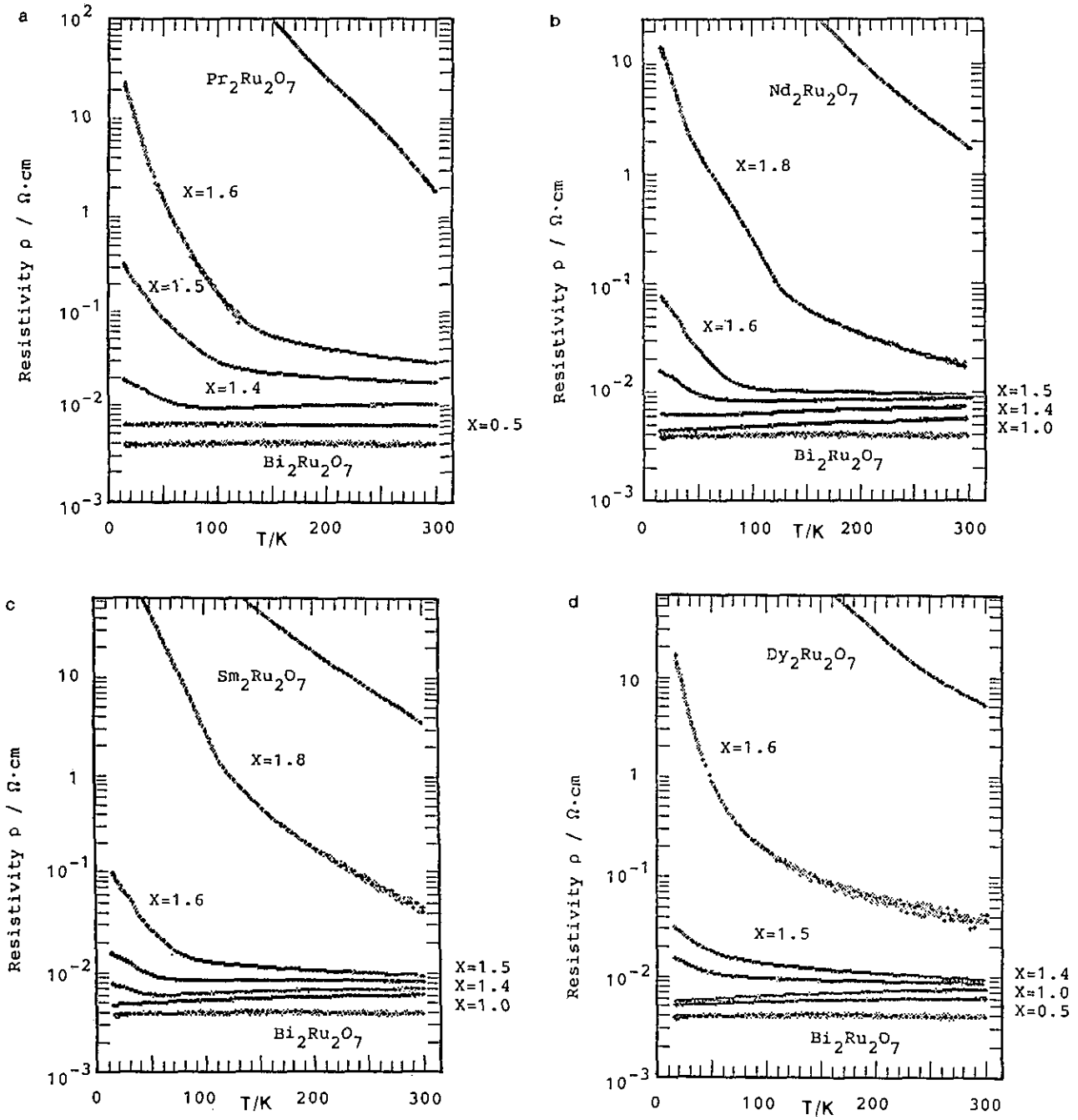

FIG. 2. Temperature dependence of resistivity for (a) $Bi_{2-x}Pr_xRu_2O_7$, (b) $Bi_{2-x}Nd_xRu_2O_7$, (c) $Bi_{2-x}Sm_xRu_2O_7$, and (d) $Bi_{2-x}Dy_xRu_2O_7$.

$x = 1.5$ $Bi_{2-x}Gd_xRu_2O_7$, which is due to a large effective ionic radius of Bi^{3+} ion (18). However, the narrow two-phase region of $1.5 < x < 1.6$ reported for $Bi_{2-x}Gd_xRu_2O_7$ (17) was not observed by our XRD measurements. No extra XRD peaks due to oxygen-vacancy ordering (21) were found.

Electrical Properties

The temperature dependence of the resistivity is shown in Fig. 2 for $Bi_{2-x}Pr_xRu_2O_7$, $Bi_{2-x}Nd_xRu_2O_7$, $Bi_{2-x}Sm_xRu_2O_7$, and $Bi_{2-x}Dy_xRu_2O_7$. $Bi_2Ru_2O_7$ is metallic, while $Ln_2Ru_2O_7$ (Ln = Pr, Nd, Sm, Dy) showed semiconducting behavior with a room-temperature resistivity of $\rho = 10^1$ Ω-cm. In the quaternary system, $Bi_{2-x}Ln_xRu_2O_7$, the resistivities increase with x, and a change from metallic to semiconducting behavior is observed between $x = 1.2$ and 1.6 for $Bi_{2-x}Ln_xRu_2O_7$ (Ln = Pr–Dy). In the previous study on $Bi_{2-x}Gd_xRu_2O_7$, the metal–nonmetal transition was observed at $x \approx 1.5$ (17, 18), which is consistent with the above data.

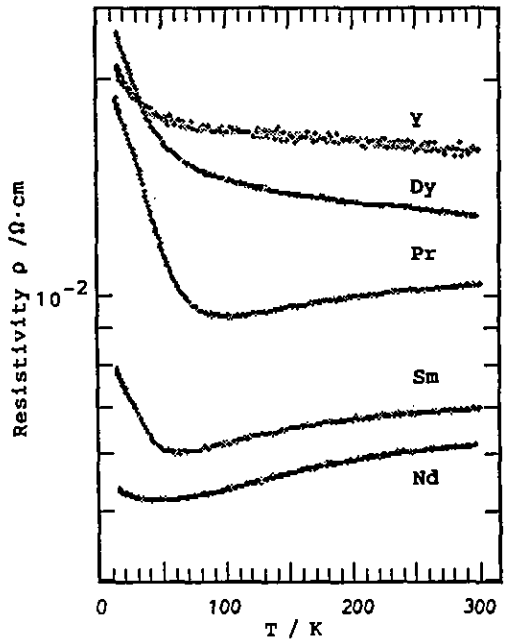

FIG. 3. Temperature dependence of resistivity for $Bi_{0.6}Ln_{1.4}Ru_2O_7$.

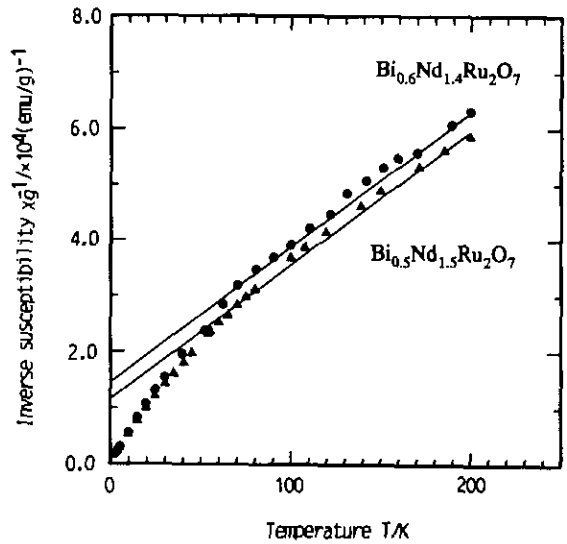

FIG. 5. Inverse magnetic susceptibility χ^{-1} vs temperature for $Bi_{2-x}Nd_xRu_2O_7$ (x = 1.4 and 1.5).

Figure 3 shows the temperature dependence of the resistivity for $Bi_{0.6}Ln_{1.4}Ru_2O_7$ with Ln = Pr–Dy, and Y. The data for Ln = Y are taken from the previous study (13). The change from semiconducting to metallic behavior is observed at 40–80 K for the composition $Bi_{0.6}Ln_{1.4}Ru_2O_7$ (Ln = Pr, Nd, Sm), which is situated between the metallic and semiconducting compositional regions. The resistivity data for $Bi_{2-x}Nd_xRu_2O_7$ in the interval of $1.4 \leq x \leq 1.6$ are plotted in Fig. 4, together with those for $Bi_{0.4}Y_{1.6}Ru_2O_7$. The resistivity curves show smooth slope changes from metallic to semiconducting behavior with a transition temperature lowering from 80 K (x = 1.6) to 40 K (x = 1.4) for $Bi_{2-x}Nd_xRu_2O_7$. Figure 1 indicates the composition region where these changes were observed. This behavior was clearly observed for the systems with larger Ln^{3+} ions (Pr, Nd). No anomalies in resistivity curves were observed for the systems with smaller Ln^{3+} ions (Dy, Y). Since the metallic behavior of $Bi_2Ru_2O_7$ is attributed to the contribution of Bi 6p orbitals (17, 18), the substitution of Ln^{3+} ions for Bi^{3+} ions decreases their contribution to the Ru 4d conduction band, and finally leads to the semiconducting behavior around x = 1.4. The composition region of 1.2–1.6 is borderline between metallic and semiconducting character; the solid solutions with Ln = Dy and Lu show semiconducting behavior, whereas Ln = Pr and Nd have metallic properties above 80 K. The inductive effect might explain the more metallic character of the pyrochlore with larger Ln^{3+} cations (22); the Ln^{3+} ion competes with the Ru^{4+} ion and withdraws electron density from the Ru–O π bonding network. The magnitude of this effect increases as the size or the basicity of the Ln^{3+} ion decreases, leading to a more semiconducting character for smaller Ln^{3+} pyrochlores.

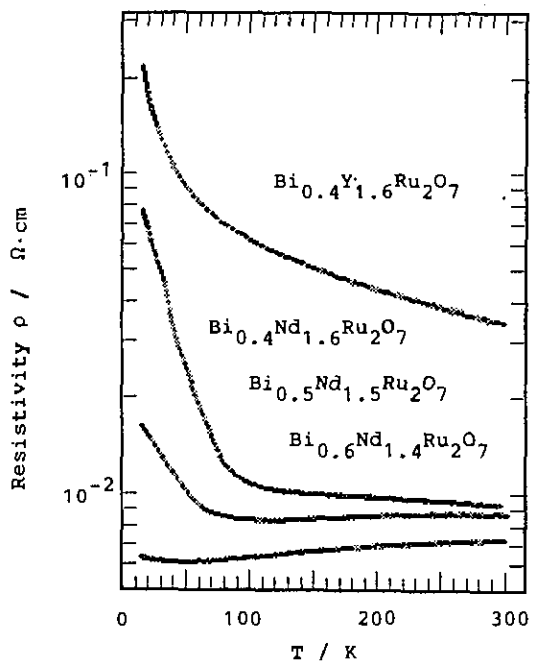

FIG. 4. Temperature dependence of resistivity for $Bi_{2-x}Nd_xRu_2O_7$ (x = 1.4–1.6) and $Bi_{0.4}Y_{1.6}Ru_2O_7$.

Magnetic Properties

Figure 5 shows the temperature dependence of the inverse magnetic susceptibility for $Bi_{2-x}Nd_xRu_2O_7$ (x = 1.4

TABLE 1
Magnetic Data for $(Bi_{2-x}Nd_x)Ru_2O_7$

Composition (x)	χ_g 200 K (emu/g)	χ_m 200 K (emu/mol)	Θ_K (K)	C_{exp} (emu/mol K)	V_{theor} (emu/mol K)		
					$C(2Nd_xRu)$	$C(2Nd_xRu)$	$C(2Nd_x)$
1.4	1.58×10^{-5}	1.02×10^{-2}	−64	2.65	4.30	5.30	2.30
1.5	1.70×10^{-5}	1.08×10^{-2}	−59	2.76	4.46	5.46	2.46

and 1.5). The Curie–Weiss constants extracted from the paramagnetic data are shown in Table 1. The Curie constants, C, are compared with two calculated models, C(2NdRu) which includes contributions from the free-ion value for Nd(III) and the spin only value for Ru(IV) ($4d^5$) and C(2Nd) which includes the Nd(III) contribution only. In all cases, the experimental C lies slightly below the C(2Nd) value. A similar result was reported in Ref. (23) and probably means that the upper temperature boundary of the data is not sufficiently high to permit the observation of the full free-ion values for either the Nd(III) or Ru(IV) contributions. A negative Weiss constant Θ is found. If the major part of Θ is determined by exchange effects, this indicates an antiferromagnetic net exchange interaction.

Crystal Structure

Crystal structure was refined for the solid solutions, $Bi_{2-x}Ln_xRu_2O_7$ (Ln = Pr, Nd, Sm, Dy), $Bi_{0.5}Gd_{1.5}Ru_2O_7$, and $Bi_{0.5}Lu_{1.5}Ru_2O_7$. Refinement of the structure proceeded with space group $Fd3m$. Initial coordinates were taken as follows: Bi(Ln), 16d(5/8, 5/8, 5/8); Ru, 16c (1/8, 1/8, 1/8); O(1), 48f (x, 0, 0), $x \approx 0.2$; O(2), 8b (1/2, 1/2, 1/2). The refinement was done in stages with the atomic coordinates and thermal parameters held fixed in the initial calculations and subsequently allowed to vary only after the scale, background, halfwidth, and unit-cell parameters were close to convergence to their optimum values. The site-occupation parameters for Bi/Ln atoms on the 16d site were fixed at the value of the starting composition. During the later refinements, when temperature factors were refined, the B_{eq}'s for the O(1) and O(2) sites had to be constrained to the same value, otherwise the refinement was unstable. In the final refinement, a total of 19 positional, thermal, and instrumental parameters were refined. The results for $Bi_{2-x}Ln_xRu_2O_7$ are summarized in Table 2. For definition of R-factors, see Ref. (19). Table 3 lists selected interatomic distances and bond angles.

Figures 6 and 7 show, respectively, the composition dependence of the interatomic distances and angles in the $Bi_{2-x}Ln_xRu_2O_7$ (Ln = Pr, Nd, Sm, Dy) systems. The interesting features of these figures are Ru–O(1) and Bi(Ln)–O(1) variations. For $Bi_{2-x}Ln_xRu_2O_7$ (Ln = Pr, Nd), the lattice parameters, Ru–O(I), and Bi(Ln)–O(2) bond lengths increase with increasing x throughout the whole composition range, whereas the Bi(Ln)–O(1) bond length decreases with x. The decrease in the Bi(Ln)–O(1) bond length is inconsistent with the lattice parameter change. For $Bi_{2-x}Ln_xRu_2O_7$ (Ln = Sm, Dy), the lattice parameters, Bi(Ln)–O(1), and Bi(Ln)–O(2) bond lengths decrease with increasing x throughout the whole composition range. However, the Ru–O(1) bond length increases with x, which is not expected from the decrease in lattice parameter. The Ru–O(1)–Ru angles decrease with x from 139° (x = 0.0) to 133.8° (x = 2.0) for Ln = Pr, and from 139° (x = 0.0) to 130° (x = 2.0) for Ln = Dy, respectively. The O(1)–Ru–O(1) angles vary with x from 88.1 and 91.2° (x = 0.0) to 85.0 and 95.0° (x = 2.0) for Ln = Pr, and to 82.6 and 97.4° (x = 2.0) for Ln = Dy, respectively. The structure refinement results are summarized as follows: the Ru–O bond length increases, the distortion of the RuO_6 octahedra increases, and the bend in the RuO_6 zigzag chains increases in the interval $0 \leq x \leq 2.0$. The bond lengths and angles vary in a similar manner for all these systems, although the lattice parameters increase for large Ln^{3+} (Pr, Nd), and decrease for small Ln^{3+} (Sm, Dy) in $Bi_{2-x}Ln_xRu_2O_7$. The transition from semiconducting to metallic behavior between x = 1.2 and 1.4 in $Bi_{2-x}Ln_xRu_2O_7$ is closely correlated with the structural variations indicated above. The pyrochlore structure consists of a framework of corner-sharing RuO_6 octahedra linked into zigzag chains (24). The substitution of Ln^{3+} for Bi^{3+} leads to the distortion of RuO_6 octahedra, the elongated Ru–O bond length, and the reduction of the Ru–O–Ru angles, which should reduce the Ru–O(1) overlap integrals and affect the electrical properties.

The compositional region of 1.2–1.6 is situated borderline between localized and itinerant Ru–4d electronic character. Figure 8 shows the variation of the bond lengths and angles in $Bi_{0.5}Ln_{1.5}Ru_2O_7$ (Ln = Pr–Lu) as a function of ionic radii for rare earth ions. The bond lengths, Ru–O(1), A–O(1), and A–O(2) increase monotonically with increasing ionic radii. The Ru–O–Ru angles increase and the splittings of O–Ru–O angles decrease with increasing ionic radii of the rare earth ions. The room temperature resistivity data show the metal–semiconducting boundary between Ln = Sm and Eu, which corresponds to the

TABLE 2
Rietveld Refinement Results for $Bi_{2-x}Ln_xRu_2O_7$

(a) $Bi_{2-x}Pr_xRu_2O_7$

Composition, x	$x = 0.0$	$x = 0.2$	$x = 0.5$	$x = 0.6$
Lattice parameter, a (Å)	10.2934(1)	10.3037(1)	10.3190(1)	10.3217(1)
x parameter	0.190(6)	0.194(6)	0.197(6)	0.196(5)
B(Bi, Pr) (Å^2)	0.9(2)	0.5(1)	0.4(1)	0.5(1)
B(Ru) (Å^2)	0.1	0.5(1)	0.4(1)	0.5(1)
B(O) (Å^2)	0.5(17)	2.0(18)	1.6(17)	1.8(15)
R_{wp}	12.58	15.75	16.50	13.95
R_p	8.96	11.47	12.09	9.85
R_e	3.59	3.78	4.04	3.87
R_I	1.94	5.36	5.98	4.75
R_F	3.27	7.73	7.59	6.63
Composition, x	$x = 1.0$	$x = 1.2$	$x = 1.4$	$x = 1.5$
Lattice parameter, a (Å)	10.3362(1)	10.3489(1)	10.3554(1)	10.3565(1)
x parameter	0.196(5)	0.198(6)	0.199(4)	0.199(4)
B(Bi, Pr) (Å^2)	0.5(1)	0.1(1)	0.2(1)	0.1(1)
B(Ru) (Å^2)	0.5(1)	0.1	0.2(1)	0.1(1)
B(O) (Å^2)	1.8(14)	1.0(13)	0.5(12)	0.4(11)
R_{wp}	13.62	15.08	15.07	14.11
R_p	9.92	10.98	10.95	9.48
R_e	3.63	4.67	3.94	4.12
R_I	4.07	4.42	3.97	3.40
R_F	6.05	5.49	4.72	4.55
Composition, x	$x = 1.6$	$x = 2.0$		
Lattice parameter, a (Å)	10.3619(1)	10.3714(1)		
x parameter	0.201(4)	0.201(4)		
B(Bi, Pr) (Å^2)	0.3(1)	0.2(1)		
B(Ru) (Å^2)	0.3(1)	0.2(1)		
B(O) (Å^2)	0.8(10)	0.1(8)		
R_{wp}	13.40	12.50		
R_p	9.28	8.92		
R_e	3.92	3.67		
R_I	3.46	2.27		
R_F	4.29	3.70		

(b) $Bi_{2-x}Nd_xRu_2O_7$

Composition, x	$x = 0.0$	$x = 0.2$	$x = 0.5$	$x = 0.8$
Lattice parameter, a (Å)	10.2934(1)	10.2988(1)	10.3058(1)	10.3142(1)
x parameter	0.190(6)	0.192(6)	0.193(5)	0.196(5)
B(Bi, Nd) (Å^2)	0.9(2)	0.9(2)	0.8(2)	0.8(2)
B(Ru) (Å^2)	0.1	0.1(3)	0.1(3)	0.1(3)
B(O) (Å^2)	0.5(17)	0.4(16)	0.2(15)	1.0(15)
R_{wp}	12.58	15.40	14.62	14.08
R_p	8.96	11.53	10.81	10.39
R_e	3.59	3.63	3.57	3.61
R_I	1.94	4.16	4.04	3.32
R_F	3.27	4.87	4.55	4.04
Composition, x	$x = 1.0$	$x = 1.2$	$x = 1.4$	$x = 1.5$
Lattice parameter, a (Å)	10.3188(1)	10.3260(1)	10.3311(1)	10.3306(1)
x parameter	0.196(5)	0.199(4)	0.198(5)	0.200(4)
B(Bi, Nd) (Å^2)	0.8(2)	0.4(2)	0.5(2)	0.1(2)
B(Ru) (Å^2)	0.2(3)	0.1(2)	0.1(2)	0.1(2)
B(O) (Å^2)	1.0(15)	0.5(13)	0.7(14)	0.2(11)
R_{wp}	13.52	14.41	10.84	13.26
R_p	10.22	10.61	8.30	9.57
R_e	3.58	3.97	3.15	3.55
R_I	2.91	3.21	5.18	2.73
R_F	4.24	4.48	8.75	3.56

TABLE 2—*Continued*

Composition, x	$x = 1.6$	$x = 1.8$	$x = 2.0$	
Lattice parameter, a (Å)	10.3341(1)	10.3311(1)	10.3362(1)	
x parameter	0.201(4)	0.202(4)	0.203(4)	
B(Bi, Nd) (Å^2)	0.2(1)	0.1(1)	0.0(1)	
B(Ru) (Å^2)	0.2(1)	0.1(1)	0.0(1)	
B(O) (Å^2)	1.0(11)	0.9(10)	0.4(10)	
R_{wp}	13.84	12.62	13.58	
R_p	10.04	8.93	9.68	
R_e	4.08	3.73	3.71	
R_I	2.75	2.18	2.25	
R_F	3.35	3.01	3.24	
	(c) $Bi_{2-x}Sm_xRu_2O_7$			
Composition, x	$x = 0.0$	$x = 0.2$	$x = 0.5$	$x = 1.0$
Lattice parameter, a (Å)	10.2934(1)	10.2948(1)	10.2921(1)	10.2902(1)
x parameter	0.190(6)	0.191(5)	0.198(6)	0.198(4)
B(Bi, Sm) (Å^2)	0.9(2)	1.2(2)	0.5(2)	0.7(2)
B(Ru) (Å^2)	0.1	0.1(3)	0.5(2)	0.1(2)
B(O) (Å^2)	0.5(17)	0.9(16)	1.9(18)	0.6(13)
R_{wp}	12.58	14.91	16.44	13.87
R_p	8.96	10.87	11.87	10.16
R_e	3.59	3.88	3.91	3.92
R_I	1.94	3.75	5.04	3.02
R_F	3.27	4.57	6.83	3.62
Composition, x	$x = 1.2$	$x = 1.4$	$x = 1.5$	$x = 1.6$
Lattice parameter, a (Å)	10.2888(1)	10.2862(1)	10.2802(1)	10.2831(1)
x parameter	0.200(4)	0.201(4)	0.201(4)	0.202(4)
B(Bi, Sm) (Å^2)	0.5(1)	0.2(1)	0.1(1)	0.3(2)
B(Ru) (Å^2)	0.5(1)	0.2(1)	0.1(1)	0.3(2)
B(O) (Å^2)	1.5(13)	1.0(12)	0.8(11)	0.9(12)
R_{wp}	13.63	13.53	13.53	14.28
R_p	10.03	9.85	9.92	10.51
R_e	3.70	3.69	3.66	3.92
R_I	3.42	3.17	3.24	2.91
R_F	4.38	3.96	3.91	3.52
Composition, x	$x = 1.8$	$x = 2.0$		
Lattice parameter, a (Å)	10.2779(1)	10.2732(1)		
x parameter	0.204(4)	0.204(4)		
B(Bi, Sm) (Å^2)	0.3(2)	0.2(2)		
B(Ru) (Å^2)	0.1(2)	0.1(2)		
B(O) (Å^2)	0.4(10)	0.4(1)		
R_{wp}	12.87	13.01		
R_p	9.30	9.58		
R_e	4.60	3.83		
R_I	2.05	2.16		
R_F	2.88	3.04		
	(d) $Bi_{2-x}Dy_xRu_2O_7$			
Composition, x	$x = 0.0$	$x = 0.2$	$x = 0.5$	$x = 0.6$
Lattice parameter, a (Å)	10.2934(1)	10.2839(1)	10.2659(1)	10.2649(1)
x parameter	0.190(6)	0.193(6)	0.197(5)	0.195(4)
B(Bi, Dy) (Å^2)	0.9(2)	0.6(2)	0.3(2)	1.1(2)
B(Ru) (Å^2)	0.1	0.6(2)	0.3(2)	0.2(2)
B(O) (Å^2)	0.5(17)	1.7(17)	1.5(15)	0.8(12)
R_{wp}	12.58	15.16	14.58	11.26
R_p	8.96	10.97	10.51	7.79
R_e	3.59	3.68	3.83	3.32
R_I	1.94	5.30	4.56	3.34
R_F	3.27	7.36	6.43	4.50

TABLE 2—*Continued*

Composition, x	$x = 1.0$	$x = 1.4$	$x = 1.5$	$x = 1.6$
Lattice parameter, a (Å)	10.2398(1)	10.2016(1)	10.2016(1)	10.1931(1)
x parameter	0.197(4)	0.203(3)	0.204(3)	0.205(4)
B(Bi, Dy) (Å^2)	0.6(2)	0.2(1)	0.2(1)	0.2(1)
B(Ru) (Å^2)	0.2(2)	0.2(1)	0.2(1)	0.2(1)
B(O) (Å^2)	0.8(11)	0.5(9)	0.4(9)	0.5(10)
R_{wp}	11.57	11.47	11.16	13.81
R_p	7.48	8.50	8.29	10.17
R_e	3.72	3.53	3.53	3.99
R_I	2.52	3.07	2.46	2.81
R_F	3.96	4.47	3.91	3.53
Composition, x	$x = 1.8$	$x = 2.0$		
Lattice parameter, a (Å)	10.1798(1)	10.1625(1)		
x parameter	0.206(4)	0.207(4)		
B(Bi, Dy) (Å^2)	0.2(2)	0.2(2)		
B(Ru) (Å^2)	0.1(2)	0.1(2)		
B(O) (Å^2)	0.6(12)	0.5(10)		
R_{wp}	12.62	12.74		
R_p	9.06	9.50		
R_e	3.75	4.10		
R_I	2.45	2.11		
R_F	4.02	3.29		

(e) $Bi_{0.5}Ln_{1.5}Ru_2O_7$

Composition	$Bi_{0.5}Lu_{1.5}Ru_2O_7$	$Bi_{0.5}Gd_{1.5}Ru_2O_7$
Lattice parameter, a (Å)	10.1187(1)	10.2468(1)
x parameter	0.205(3)	0.204(4)
B(Bi, Ln) (Å^2)	0.31(9)	0.1(2)
B(Ru) (Å^2)	0.31(9)	0.3
B(O) (Å^2)	0.4(7)	0.7(13)
R_{wp}	9.02	15.52
R_p	6.24	11.32
R_e	3.27	4.21
R_I	2.35	3.79
R_F	2.68	4.51

above structural variations that increase in Ru–O(1)–Ru angle and decrease in RuO_6 octahedra distortion with the size of Ln^{3+} ions. The geometric effect is therefore an important factor for the metal–semiconducting change across the rare earth series.

CONCLUSIONS

We synthesized the $Bi_{2-x}LnRu_2O_7$ solid solution with the pyrochlore structure for Ln = Pr–Lu. The resistivity increases with x, and a change from metallic to semicon-

TABLE 3
Selected Bond Lengths (Å) and Angles (°) for $Bi_{2-x}Ln_xRu_2O_7$

	$Bi_2Ru_2O_7$	$Pr_2Ru_2O_7$	$Nd_2Ru_2O_7$	$Sm_2Ru_2O_7$	$Dy_2Ru_2O_7$
Ln–O(1)	2.63(5)	2.58(3)	2.55(3)	2.52(3)	2.48(3)
Ln–O(2)	2.2286(1)	2.24547(1)	2.2379(1)	2.2242(1)	2.20025(1)
Ru–O(1)	1.94(2)	1.993(14)	1.996(16)	1.991(18)	1.981(16)
O(1)–Ru–O(1)	91.2(19)	95.0(9)	95.8(10)	96.5(11)	97.4(9)
	88.8(19)	85.0(9)	84.2(10)	83.5(11)	82.6(9)
Ru–O(1)–Ru	139(4)	133.8(19)	132(2)	132(2)	130(2)
Ln–O(1)–Ln	88.5(2)	90.7(11)	91.5(13)	92.0(14)	93.0(13)

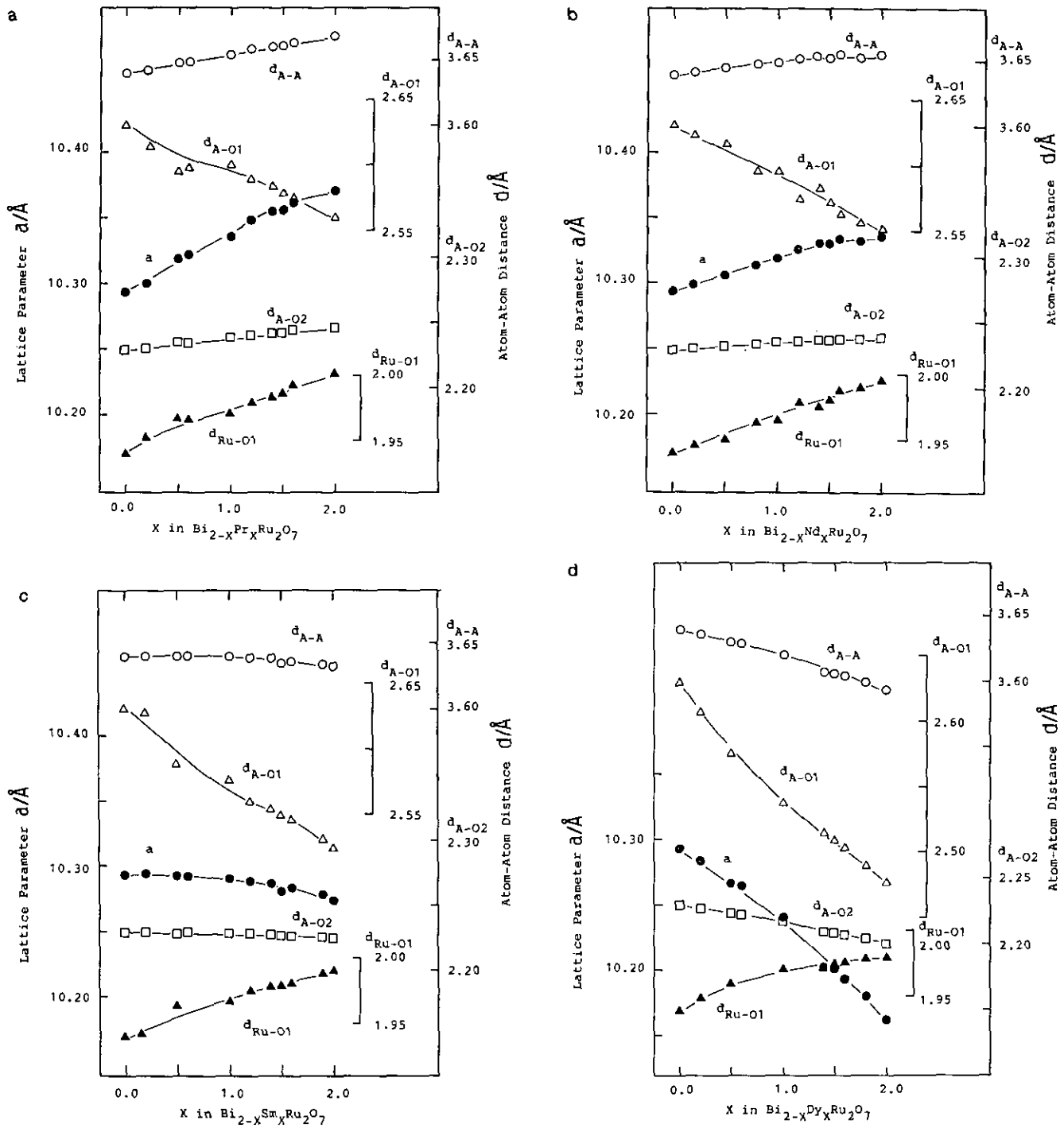

FIG. 6. Variation of the bond lengths in (a) $Bi_{2-x}Pr_xRu_2O_7$, (b) $Bi_{2-x}Nd_xRu_2O_7$, (c) $Bi_{2-x}Sm_xRu_2O_7$, and (d) $Bi_{2-x}Dy_xRu_2O_7$.

ducting behavior is observed between $x = 1.2$ and 1.4. The structure refinement results are summarized as follows: With increasing Ln^{3+} contents, the lattice parameters in $Bi_{2-x}Ln_xRu_2O_7$ increase for Ln = Pr and Nd and decrease for Ln = Sm and Dy. However, in all Ln series, (i) the Ru–O bond lengths increase, (ii) the distortion of the RuO_6 octahedra increases, and (iii) the bend in the RuO_6 zigzag chains increases in the interval $0 \leq x \leq 2.0$. The above structural changes reduce the Ru–O–Ru interaction with increasing x. The distortion of the RuO_6 octahedra and the bend in the RuO_6 zigzag chains increase also in the order Lu → Pr, leading to the metallic–

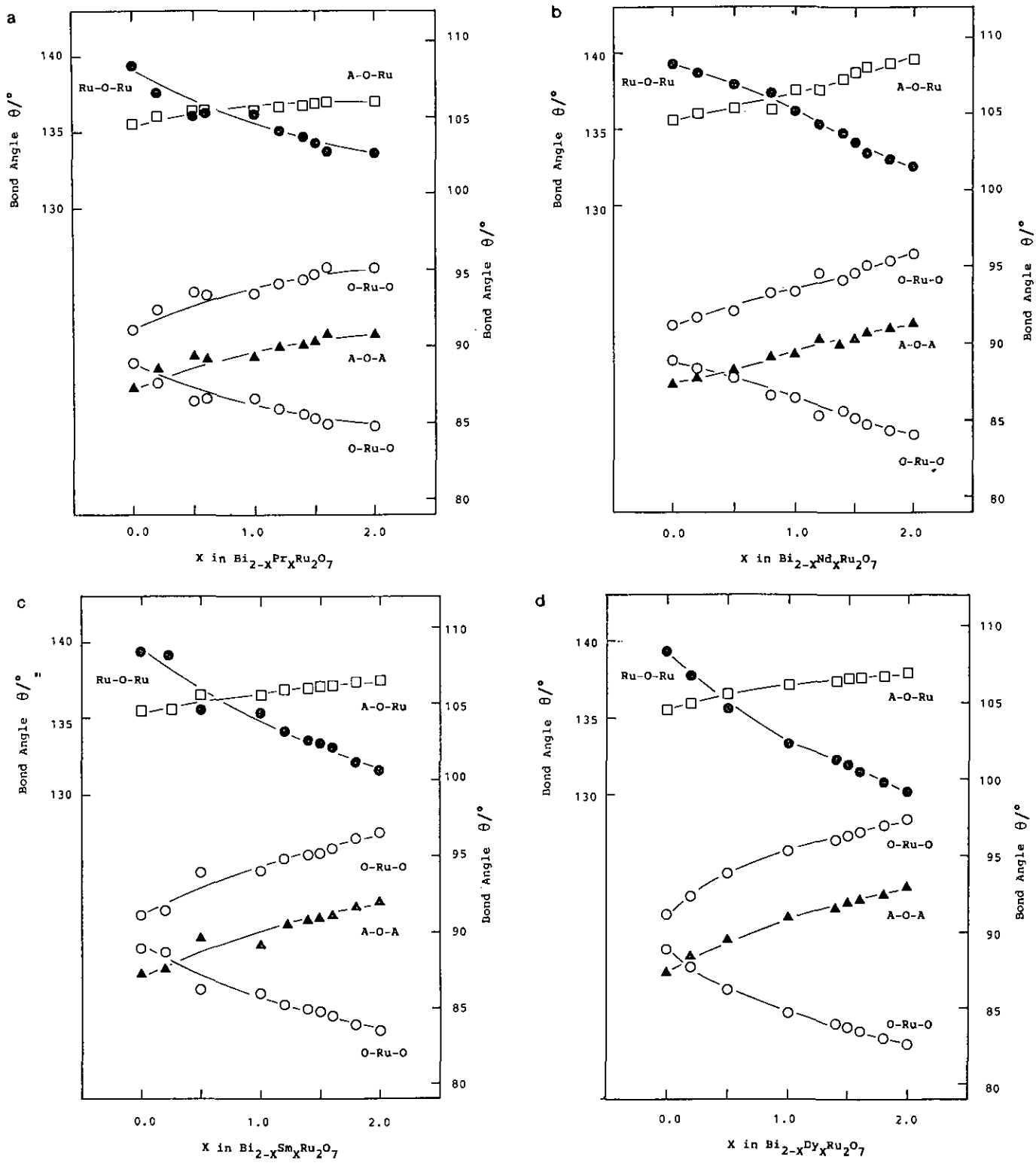

FIG. 7. Variation of the bond angles in (a) $Bi_{2-x}Pr_xRu_2O_7$, (b) $Bi_{2-x}Nd_xRu_2O_7$, (c) $Bi_{2-x}Sm_xRu_2O_7$, and (d) $Bi_{2-x}Dy_xRu_2O_7$.

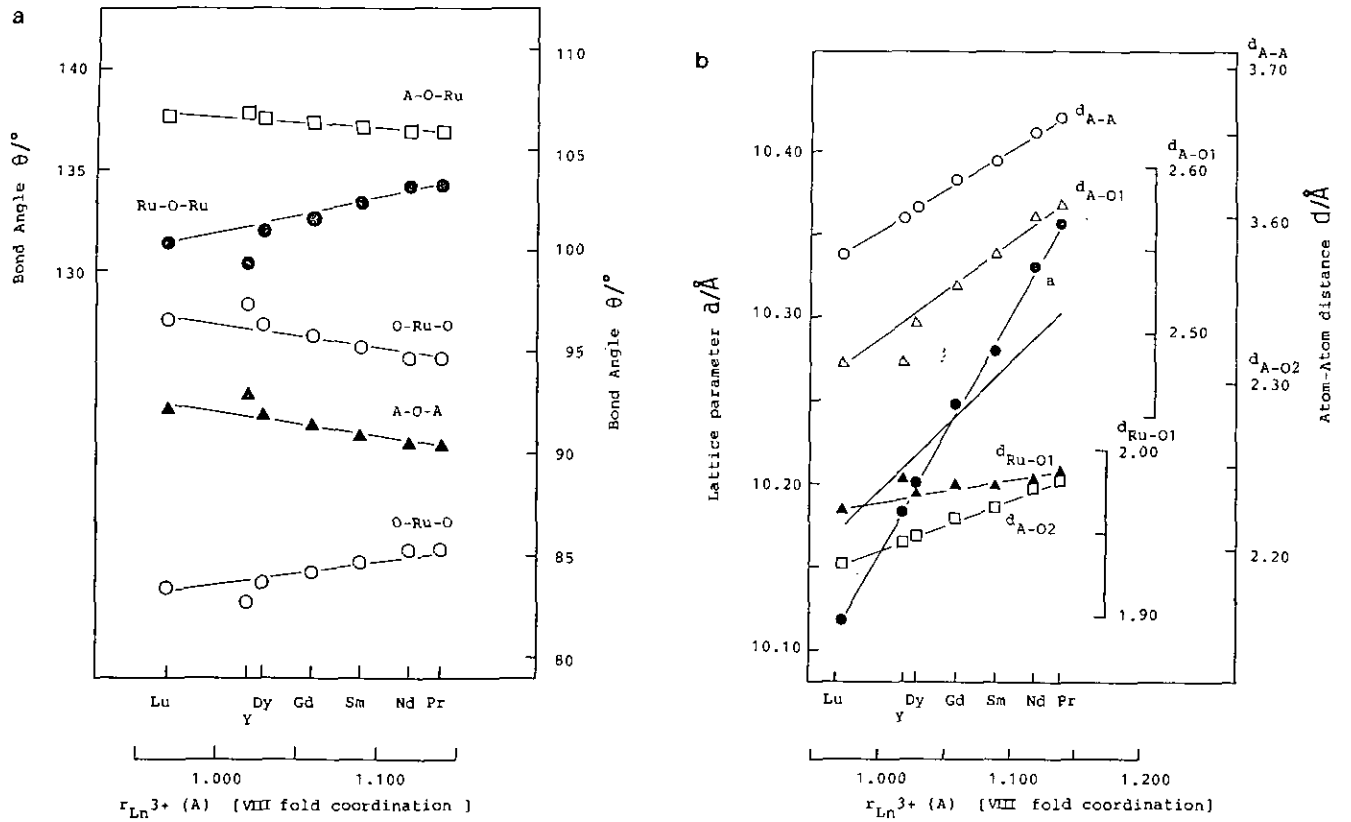

FIG. 8. Variation of the (a) bond lengths and (b) angles in $Bi_{0.5}Ln_{1.5}Ru_2O_7$.

semiconducting boundary between Sm and Eu in $Bi_{0.5}Ln_{1.5}Ru_2O_7$ above 100 K. The metallic temperature dependence changes to semiconducting below 40–80 K for Ln = Pr–Sm in $Bi_{2-x}Ln_xRu_2O_7$ (x = 1.4–1.6). Finally, the technique of X-ray Rietveld refinement provides a convenient and powerful probe into the structural variations of the pyrochlore solid solutions.

ACKNOWLEDGMENTS

We thank Dr. F. Izumi of NIRIM for providing the computer program RIETAN. All computations for structure determination were carried out at the Mie University Information Processing Center. We gratefully acknowledge support from the Tokuyama Science Foundation. This work was supported partly by a grant-in-aid for Scientific Research on Chemistry of New Super Conductors from the Ministry of Education, Science and Culture.

REFERENCES

1. A. T. Ashcroft, A. K. Cheetham, J. S. Foord, M. L. H. Green, C. P. Grey, A. J. Murrell, and P. D. F. Vernon, *Nature* **344,** 319 (1990).
2. R. G. Egdell, J. B. Goodenough, A. Hamnett, and C. C. Naish, *J. Chem. Soc., Faraday Trans. 1* **79,** 893 (1983).
3. G. E. Pike and C. H. Seager, *J. Appl. Phys.* **48,** 5152 (1977).
4. P. F. Carcia, A. Ferreti, and A. Suna, *J. Appl. Phys.* **53,** 5282 (1982).
5. N. Sinnadurai and K. J. Wilson, *IEEE Trans. Compon., Hybrids, Manuf. Technol.* **CHMT-5,** 308 (1982).
6. R. J. Bouchard and J. L. Gillson, *Mater. Res. Bull.* **6,** 669 (1971).
7. J. M. Longo, P. M. Raccah, and J. B. Goodenough, *Mater. Res. Bull.* **4,** 191 (1969).
8. R. Aleonard, A. F. Berthand, M. C. Montmory, and R. Pauthenet, *J. Appl. Phys.* **33,** 1205 (1962).
9. W. Y. Hsu, R. V. Kasowski, T. Miller, and T.-C. Chiang. *Appl. Phys. Lett.* **52,** 792 (1988).
10. Y. Takeda, R. Kanno, M. Sakano, O. Yamamoto, M. Takano, Y. Bando, H. Akinaga, K. Takita, and J. B. Goodenough, *Mater. Res. Bull.* **25,** 293 (1990).
11. Y. Takeda, M. Nishijima, N. Imanishi, R. Kanno, O. Yamamoto, and M. Takano, *J. Solid State Chem.* **96,** 72 (1992).
12. R. Kanno, Y. Kawamoto, Y. Takeda, M. Hasegawa, O. Yamamoto, and N. Kinomura, *J. Solid State Chem.* **96,** 397 (1992).
13. R. Kanno, Y. Takeda, T. Yamamoto, Y. Kawamoto, and O. Yamamoto, *J. Solid State Chem.* **102,** 106 (1993).
14. J. E. Greedan, M. Sato, N. Ali, and W. R. Datars, *J. Solid State Chem.* **68,** 300 (1987).
15. A. W. Sleight and R. J. Bouchard, "National Bureau of Standards Special Publication 364, Solid State Chemistry, Proceedings, 5th Materials Research Symposium," p. 227, 1972.
16. A. Ehmann and S. Kemmler-Sack, *Mater. Res. Bull.* **20,** 437 (1985).
17. J. B. Goodenough, A. Hamnett, and D. Telles, "Localization and Metal-Insulator Transition," (H. Fritzsche and D. Adler, Eds.). Plenum, New York, 1985.
18. P. A. Cox, J. B. Goodenough, P. J. Tavener, D. Telles, and R. G. Egdell, *J. Solid State Chem.* **62,** 360 (1986).

19. F. Izumi, "The Rietveld Method" (R. A. Young, Ed.), Chap. 13. Oxford Univ. Press, Oxford, 1993.
20. R. D. Shannon and C. T. Prewitt, *Acta Crystallogr., Sect. B* **25,** 925 (1969).
21. R. A. Beyerlein, H. S. Horowitz, J. M. Longo, M. E. Leonowicz, J. D. Jorgensen, and F. J. Rotella, *J. Solid State Chem.* **51,** 253 (1984).
22. J. B. Goodenough, *Prog. Solid State Chem.* **5,** 145 (1971); M. A. Subramanian, G. Arvamudan, and G. V. Subba Rao, *Mater. Res. Bull.* **15,** 1401 (1980); M. A. Subramanian, C. C. Torardi, D. C. Johnson, J. Pannetier, and A. W. Sleight, *J. Solid State Chem.* **72,** 24 (1988).
23. M. Sato, X. Yan, and J. E. Greedan, *Z. Anorg. Allg. Chem.* **540/541,** 177 (1986).
24. M. A. Subramanian, G. Aravamdan, and G. V. Subba Rao, *Prog. Solid State Chem.* **15,** 55 (1983).